CONDENSED MATTER PHYSICS

Weyl fermions, Fermi arcs, and minority-spin carriers in ferromagnetic CoS_2

Niels B. M. Schröter[1]*†, Iñigo Robredo[2,3]*, Sebastian Klemenz[4], Robert J. Kirby[4], Jonas A. Krieger[1,5,6], Ding Pei[7], Tianlun Yu[1,,8], Samuel Stolz[9,10], Thorsten Schmitt[1], Pavel Dudin[11]‡, Timur K. Kim[11], Cephise Cacho[11], Andreas Schnyder[12], Aitor Bergara[2,3,13], Vladimir N. Strocov[1], Fernando de Juan[2,14], Maia G. Vergniory[2,14]†, Leslie M. Schoop[4]†

Copyright © 2020 The Authors, some rights reserved; exclusive licensee American Association for the Advancement of Science. No claim to original U.S. Government Works. Distributed under a Creative Commons Attribution NonCommercial License 4.0 (CC BY-NC).

Magnetic Weyl semimetals are a newly discovered class of topological materials that may serve as a platform for exotic phenomena, such as axion insulators or the quantum anomalous Hall effect. Here, we use angle-resolved photoelectron spectroscopy and ab initio calculations to discover Weyl cones in CoS_2, a ferromagnet with pyrite structure that has been long studied as a candidate for half-metallicity, which makes it an attractive material for spintronic devices. We directly observe the topological Fermi arc surface states that link the Weyl nodes, which will influence the performance of CoS_2 as a spin injector by modifying its spin polarization at interfaces. In addition, we directly observe a minority-spin bulk electron pocket in the corner of the Brillouin zone, which proves that CoS_2 cannot be a true half-metal.

INTRODUCTION

Since the experimental discovery of topological insulators and topological semimetals, there has been a substantial effort to functionalize topological materials for spintronic applications, most prominently in the family of Bismuth chalcogenides (*1*–*4*). However, because the field of spintronics predates the first prediction of topological insulators (*5*, *6*) and topological semimetals (*7*), topological phenomena in many well-studied spintronic materials may have been overlooked during initial investigations of their electronic properties. Here, we reveal that CoS_2, a material that has been long studied because of its itinerant ferromagnetism and potential for half-metallicity, actually hosts Weyl fermions and Fermi arc surface states in its band structure close to the Fermi level E_F, as well as topological nodal lines below the Fermi level. CoS_2 is, therefore, a rare example of the recently discovered class of experimentally verified magnetic topological metals (*8*–*10*), which have been proposed to realize new mechanisms of spin-to-charge conversion (*11*), and are of broader interest for fundamental science, for instance, as a platform to realize axion insulators (*7*), the intrinsic anomalous Hall effect (*12*), or the anomalous fractional quantum Hall effect (*13*).

Beyond the discovery of its topological properties, we also clarify the question of whether CoS_2 is a true half-metal. Half-metallic ferromagnets, i.e., materials that are metallic in one spin channel but gapped in the other, have been considered as promising materials for spintronic devices, where they could act as sources of highly spin-polarized charge carriers. There has been a longstanding debate on whether CoS_2 or the related alloys $Co_{1-x}Fe_xS_2$ are true half-metals, which has important implications for materials and device engineering. Calculations within the local spin density approximation (LSDA) (*14*, *15*) [see Fig. 1 (A and B)] conclude that CoS_2 hosts a minority-spin electron pocket at the R point that leads to a peak in the minority-spin density of states (DOS), which would make CoS_2 a minority-spin conductor. This scenario is supported by magnetotransport experiments that suggest a sign flip in the spin polarization upon hole doping with iron that may turn CoS_2 into a half-metal (i.e., vanishing minority-spin DOS at E_F) due to the depopulation of a minority-spin electron pocket (*16*–*20*). On the other hand, calculations based on the generalized gradient approximation (GGA) (*15*, *21*) [see Fig. 1 (B and C)] conclude that half-metallicity is already obtained in the undoped compound, and quantum oscillation experiments were unable to detect the putative minority-spin electron pocket (*21*). To resolve the debate about the half-metallicity of CoS_2, a direct spectroscopic band structure investigation would be clearly desirable, also because the spin polarization measured with transport probes can be reduced by surface defects (*22*) and can therefore not entirely rule out intrinsic half-metallicity. It should be noted that finite temperature effects can also reduce the spin polarization of nominally half-metallic ferromagnets (*23*).

Besides the bulk band structure, electronic surface states also influence the spin polarization at the Fermi level, which becomes particularly important for heterostructure interfaces in spintronic devices where half-metals could function as spin injectors. One important class of surface states are topological Fermi arcs in Weyl semimetals, which are considered to be particularly robust against passivation due to the protection by topological bulk invariants. Our LSDA calculations of CoS_2 shown in Fig. 1 (A and B) predict Weyl nodes close to the Fermi level on the $k_x = 0$ and $k_y = 0$ planes

[1]Swiss Light Source, Paul Scherrer Institute, CH-5232 Villigen PSI, Switzerland. [2]Donostia International Physics Center, 20018 Donostia-San Sebastian, Spain. [3]Condensed Matter Physics Department, University of the Basque Country UPV/EHU, 48080 Bilbao, Spain. [4]Department of Chemistry, Princeton University, Princeton, NJ 08540, USA. [5]Laboratorium für Festkörperphysik, ETH Zurich, CH-8093 Zurich, Switzerland. [6]Laboratory for Muon Spin Spectroscopy, Paul Scherrer Institute, CH-5232 Villigen PSI, Switzerland. [7]Clarendon Laboratory, Department of Physics, University of Oxford, Oxford OX1 3PU, UK. [8]Advanced Materials Laboratory, State Key Laboratory of Surface Physics and Department of Physics, Fudan University, Shanghai 200433, China. [9]EMPA, Swiss Federal Laboratories for Materials Science and Technology, 8600 Dübendorf, Switzerland. [10]Institute of Condensed Matter Physics, Station 3, EPFL, 1015 Lausanne, Switzerland. [11]Diamond Light Source, Didcot, OX110DE, UK. [12]Max Planck Institute for Solid State Research, 70569, Stuttgart, Germany. [13]Centro de Física de Materiales, Centro Mixto CSIC -UPV/EHU, 20018 Donostia, Spain. [14]IKERBASQUE, Basque Foundation for Science, Maria Diaz de Haro 3, 48013 Bilbao, Spain.

*These authors contributed equally to this work.

†Corresponding author. Email: niels.schroeter@psi.ch (N.B.M.S.); maiagvergniory@dipc.org (M.G.V.); lschoop@princeton.edu (L.M.S.)

‡Present address: Synchrotron SOLEIL, Saint-Aubin, 91192 Gif-sur-Yvette, France.

Downloaded from http://advances.sciencemag.org/ on April 17, 2021

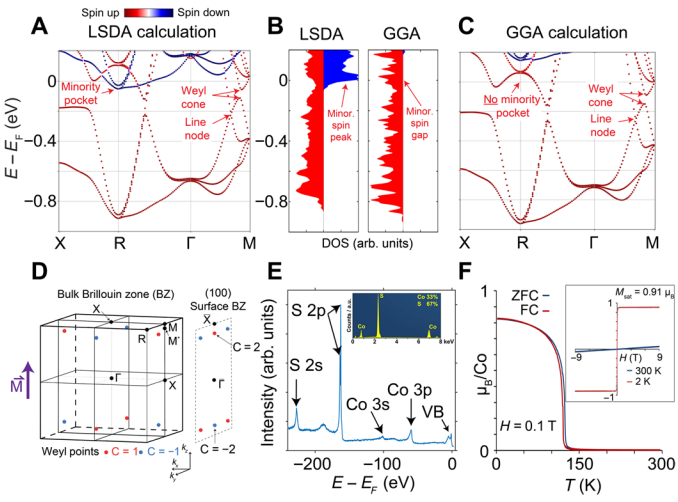

Fig. 1. Electronic structure and characterization of CoS_2 samples. (**A**) Band structure obtained from LSDA. (**B**) Comparison of DOS from both spin channels for LSDA and GGA. The red solid area shows the majority spin, and the blue solid area shows the minority spins. (**C**) Band structure obtained from GGA. (**D**) Illustration of the Weyl points in the bulk Brillouin zone, which are located on the high symmetry planes $k_x = 0$ and $k_y = 0$ parallel to the magnetization direction $\vec{M}$. Red dots indicate Weyl points with positive Chern number C; blue dots indicate Weyl points with negative Chern number. (**E**) Core-level spectroscopy measured with photon energy hv = 602 eV; arrows indicate elemental core levels and valence band (VB). Inset shows energy-dispersive x-ray spectroscopy (EDX) curves, showing an ideal stoichiometry. (**F**) Temperature dependence of magnetization curve under zero field-cooling (ZFC) and field-cooled (FC) conditions; the applied field is 0.1 T. The Curie point at 130 K is indicated. The inset shows the magnetic field dependence below and above the Curie temperature. The measurements were taken along the [100] direction.

parallel to the magnetization direction (see Fig. 1D), which should give rise to topological Fermi arc surface states. In addition, we find topological nodal lines a few hundreds of milli–electron volts below the Fermi level, which are protected by a $\{m_z|½\ 0\ ½\}$ glide operation (also see the Supplementary Materials). Since the concept of topological semimetals and Fermi arc surface states was not yet established at the time, previous theoretical studies of CoS_2 overlooked these important features in its band structure, which can have a decisive influence on spin transport properties.

Previous angle-resolved photoelectron spectroscopy (ARPES) experiments (*24*–*26*) on CoS_2 were performed with photon energies between hv = 20 to 120 eV where the inelastic mean free path of the photoelectrons can be expected to be close to its minimum ~0.5 to 1 nm, resulting in very surface sensitive probes. This implies that the signal from bulk bands is substantially broadened along the momentum direction k_z perpendicular to the sample surface (*27*), which makes the identification of any bulk band dispersion in these experiments challenging, and no minority-spin bulk electron pocket in the vicinity of the R point could be resolved. While previous studies did report the presence of surface states (*26*), it remained unclear whether these surface states are crossing the Fermi level and whether they are of topological origin.

Here, we overcome these limitations by using complementary bulk-sensitive soft x-ray ARPES (SX-ARPES; hv > 400 eV) and surface-sensitive vacuum ultraviolet ARPES (VUV-ARPES; hv < 120 eV) to disentangle the bulk and surface electronic structure of CoS_2. As a result, we are able to observe its elusive minority-spin bulk electron pocket at the R point of the Brillouin zone directly, settling the longstanding debate of half-metallicity in CoS_2. We also detect a topological line node located at ~150 meV below the Fermi level, as well as a Weyl cone that suggest a Weyl point slightly above the Fermi level, which gives rise to topological Fermi arc surface states that cross the Fermi level. By comparison with ab initio calculations, we find that these Fermi arcs are of majority spin character and therefore affect the spin polarization at a heterostructure interface.

RESULTS

Our samples were synthesized using chemical vapor transport. We studied their elemental composition with core-level spectroscopy and energy-dispersive x-ray spectroscopy, which confirmed the expected stoichiometry (see Fig. 1E). Powder x-ray diffraction confirmed the previously reported cubic space group 205 and a lattice constant of $a = 5.5287$ (*5*) (see Materials and Methods and the Supplementary Materials for more details about synthesis and characterization). We measured a Curie temperature of $Tc = 124$ K and a saturation magnetization of 0.91 μ_B/Co at 9 T (which becomes linear at 0.2 T and 0.89 μ_B), in good agreement with the literature values (*28*) (see Fig. 1F for magnetization curves). The coercivity in our data is small, about 10 to 15 Oe, which agrees also with the literature values (*16*).

When cleaving CoS_2 for ARPES experiments, we obtained two distinct cleavage planes with the surface normal pointing along the (111) and (100) directions. We performed photon energy–dependent ARPES measurements with soft x-ray photons (hv = 350 to 800 eV) to locate the high-symmetry planes along the k_z direction normal to the sample surface (see the Supplementary Materials). The band structure in the $k_z = \pi$ plane containing the R point is for the (111) surface displayed in Fig. 2 (see fig. S9 for a definition of the high-symmetry planes). We can clearly identify circular Fermi surface pockets at the R point in the corner of the Brillouin zone in Fig. 2A. Our calculated Fermi surface (Fig. 2B; using the LSDA) is in good qualitative agreement with the experimental data, confirming the existence of Fermi surface pockets at the R point. When inspecting the experimental band dispersion along the R-X-R direction (Fig. 2C), we see that the circular pockets at the R point are electron-like and are related to another parabolic band with a minimum at around ~0.65 eV by the exchange splitting. The magnitude of the exchange splitting extracted from the energy distribution curve at the R point (Fig. 2D) is $\Delta E = 0.60$ eV (3). Our LSDA calculations of the band dispersion shown in Fig. 2E are in good qualitative agreement with the experimental data and indicate that the observed electron pocket is of minority-spin character, which implies that CoS_2 is not a true half-metal. However, the experimentally observed exchange splitting is ~250 meV smaller than in the LSDA calculations, such that the majority spin bands are located closer to the Fermi level in the experiment than expected from the calculations. The data measured on the (100) surface also show electron pockets at the R point and are displayed in the Supplementary Materials.

To search for the topological nodal line and Weyl nodes in CoS_2, we also probed the bulk band structure in the $k_z = 0$ plane, containing the Γ point, as illustrated in Fig. 3. Figure 3 (A to D) displays the experimental and calculated Fermi surfaces for the (111) and (100) cleavage planes, which are in good qualitative agreement. Figure 3E shows the band dispersion along the M-Γ direction (black arrow in

Downloaded from http://advances.sciencemag.org/ on April 17, 2021

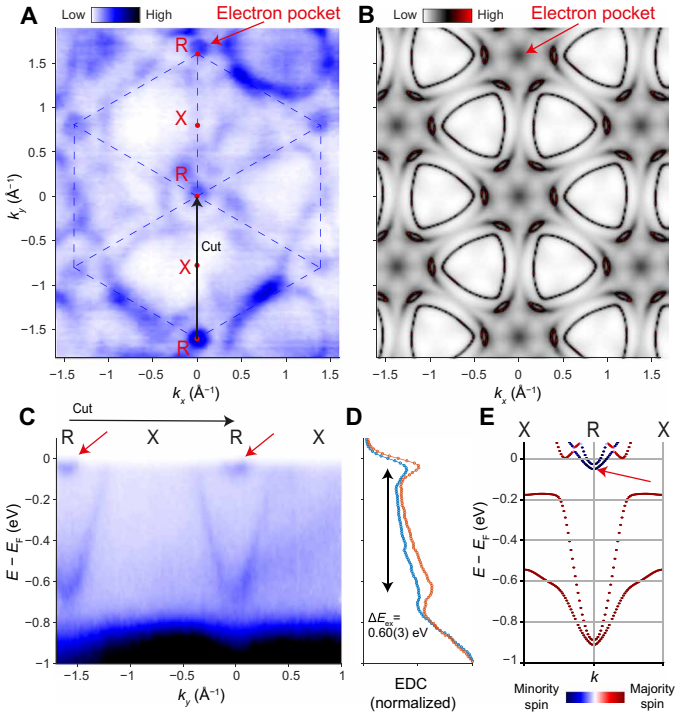

Fig. 2. Bulk band structure of the $k_z = \pi$ plane measured on the (111) surface. (**A**) Experimental Fermi surface was measured on the (111) cleavage plane with photon energy hv = 602 eV and linear-vertical polarization, integrated over 50 meV below the Fermi energy. The red arrow indicates an electron pocket located at the R point. The black arrow indicates the position of the line cut shown in (C). (**B**) Calculated Fermi surface spectral function $A(k,E_F)$ for the same plane as shown in (A) obtained with the LSDA. (**C**) Line cut along the R-X-R direction as shown in (A); red arrows indicate the electron pockets at the R point. (**D**) Energy distribution curves for the two R points shown in (E). The black arrow indicates the magnitude of the exchange splitting of $\Delta E = 0.60(3)$ eV. (**E**) Calculated band structure obtained with LSDA; red arrows indicate minority-spin electron pocket.

Fig. 3A), measured on the (111) surface (black arrow in Fig. 3A), and the Γ-M direction, measured on the (100) surface (black arrow in Fig. 3C). Note that the observable bands along these two directions are very different, possibly due to matrix element effects. The line cut obtained from the (111) surface shows a V-shaped feature centered at the M point and a quasi-parabolic band centered at the Γ point. In contrast, the dispersion obtained from the (100) surface shows a single band dispersing in the opposite direction from the quasi-parabolic band. To enhance the contrast of our data, we also show the corresponding second derivative spectrum in Fig. 3F. The combined band dispersion from both surfaces is illustrated in Fig. 3G, which displays the peak positions from a fit of the momentum distribution curves. By comparison with the calculated band dispersion shown in Fig. 3H, we can see that the band crossing between the blue and red bands [from the (111) surface and (100) surface, respectively] is part of a topological line node, while the blue bands form a Weyl cone. The Weyl point that corresponds to the Weyl cone is shown in Fig. 3I, which displays the calculated band dispersion along the M*-Γ direction, where M* $(0, 0.5, 0.4581)\frac{2\pi}{a}$ is a point that is slightly displaced from M $(0, 0.5, 0.5)\frac{2\pi}{a}$ (see Fig. 1D), which is identical to the M point within the experimental uncertainty. Since we cannot observe the band top of the blue bands along the M-Γ direction in our experimental data, we conclude that the Weyl point must be located slightly above the Fermi level.

Fermi arc surface states are a hallmark of Weyl points in topological semimetals. Therefore, the Weyl points in CoS_2 must be accompanied by Fermi arc surface states that are connecting the projections of the Weyl points in the surface Brillouin zone. We used surface-sensitive VUV-ARPES to investigate the surface electronic structure of the (100) surface in CoS_2, the results of which are displayed in Fig. 4. Figure 4A shows the experimentally obtained Fermi surface, which was measured on a strongly tilted crystal plane. The photon energy dependence of the Fermi surface maps (see the Supplementary Materials) indicates that all Fermi surface pockets measured by VUV-ARPES are surface states and that the signal from bulk states is mostly suppressed in this photon energy range. The positions of the projections of the Weyl point in the (100) surface Brillouin zone are shown in Fig. 1D. From our ab initio calculations, we expect that there should be two Weyl cone projections with total Chern numbers C = ±2 in the vicinity of the $\overline{X}$ point of the surface Brillouin zone, which originate from the Weyl cones in the vicinity of the M point of the bulk Brillouin zone that we have experimentally observed in Fig. 3 (E to G). These two Weyl points have to be connected by two Fermi arcs, which can form a circular Fermi surface (see Fig. 4B). This relationship between Weyl cone projections and topological surface states is precisely what we observe in our experimental data in Fig. 4A, which shows small circular Fermi surface pocket centered at the $\overline{X}$ point. A corresponding line cut of the experimental data along the $\overline{X} - \overline{\Gamma} - \overline{X}$ path is shown in Fig. 4C. It displays a surface state band crossing the Fermi level that connects two hole-like pockets that are located at the $\overline{X}$ points at opposite ends of the Brillouin zone. Our ab initio calculations of the surface electronic structure displayed in Fig. 4D confirm that this surface state is a Fermi arc that connects two Weyl points. Note that the renormalized energy scale of the Fermi arcs in the calculation compared to the experiment is expected owing to the reduced exchange splitting, which we already observed for the bulk band structure. Therefore, the Fermi arcs cross the Fermi level in the experiment, while they are located below the Fermi level in the calculation. Figure 4 (E to G) shows that the same line cut is measured at different photon energies, which shows that the Fermi arc dispersion is independent of the k_z momentum, which proves its two-dimensional nature. Since the Fermi arcs are derived from majority-spin bulk bands, they have majority-spin character (see the Supplementary Materials for calculations of their spin polarization). This will influence the spin polarization of electrons at the Fermi level at heterostructure interfaces where CoS_2 can act as a spin injector.

DISCUSSION

One may wonder whether the appearance of the conical bulk-band pockets connected by surface states could just be a coincidence, and whether the circular surface state pocket observed here may actually be just a trivial surface state. However, such a coincidence would require an unrealistic degree of fine-tuning, because there are no symmetry constraints that should pin a trivial surface state to the projections of the conical bulk bands. The only plausible explanation is, therefore, that the surface states mentioned above are Fermi arcs, and the observed linear bulk bands are part of a Weyl cone. Although we cannot directly observe the Weyl point since it is located

Downloaded from http://advances.sciencemag.org/ on April 17, 2021

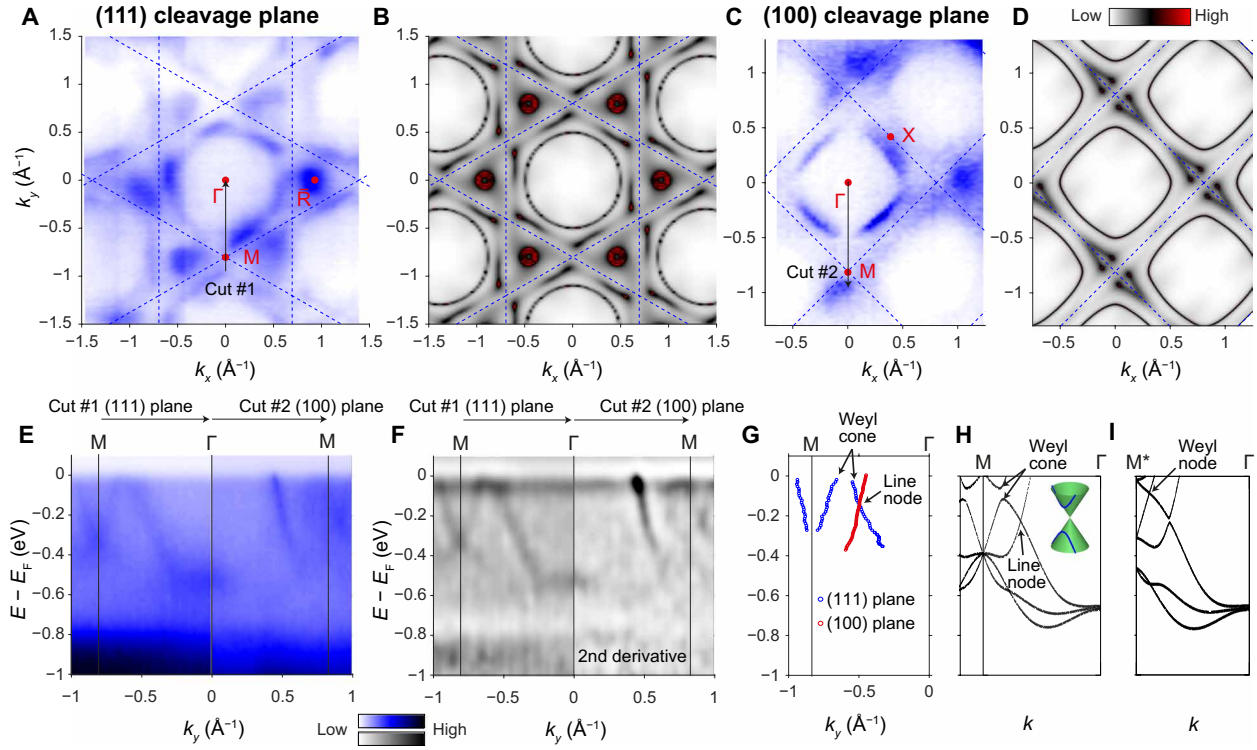

Fig. 3. Bulk band structure of the $k_z = 0$ plane. (**A**) Experimental Fermi surface measured on the (111) cleavage plane with photon energy hv = 512 eV and linear-vertical polarization, integrated over 50 meV below the Fermi energy. The black arrow indicates the position of the line cut shown in (E). (**B**) Calculated Fermi surface spectral function for the same plane as shown in (A) obtained with LSDA. (**C**) Experimental Fermi surface spectral function $A(k,E_F)$ measured on the (100) cleavage plane with photon energy hv = 475 eV and linear-vertical polarization, integrated over 50 meV below the Fermi energy. The black arrow indicates the position of the line cut shown in (E). (**D**) Calculated Fermi surface for the same plane as shown in (C) obtained with LSDA. (**E**) Line cuts along the M-Γ direction from the (111) surface, as shown in (A), and the Γ-M direction from the (100) surface, as shown in (C). (**F**) Second-derivative spectrum of (E). (**G**) Result of the momentum distribution curve (MDC) fitting of the bands along the M-Γ-M direction, where blue circles originate from data of the (111) plane, and red circles originate from data of the (100) plane. (**H**) Calculated band dispersion along the M-Γ direction. (**I**) Band dispersion along the M*-Γ direction where M* (0,0.5,0.4581)$\frac{2\pi}{a}$ is a point slightly displaced from the M point (see Fig. 1D), such that the k-path is passing through the Weyl point in the vicinity of M.

in the unoccupied part of the DOS, the overall agreement between the experimental data and LSDA calculations in conjunction with experimentally observed momentum space alignment between surface states and bulk bands provides sufficient evidence to conclude that CoS_2 is a magnetic Weyl semimetal.

Because of the relatively low effective mass of the minority-spin electron pocket at the R point, the minority-spin DOS at the Fermi level is large, and some calculations suggested that CoS_2 is a minority-spin conductor (*18*). Our discovery of the majority-spin Fermi arc surface states implies that the total interface spin polarization of a heterostructure involving CoS_2 will be reduced compared to the bulk value. Compared to trivial dangling bond surface states, Fermi arc surface states are more robust against attempts of passivation, because they are protected by the topological invariants (the Chern numbers) of the bulk Weyl points; hence, engineering of the interface potential cannot easily remove the Fermi arcs. On the other hand, hole doping with iron has been suggested to transform CoS_2 from a minority-spin to a majority-spin conductor and ultimately to a full half-metal by depopulation of the minority-spin bulk electron pocket (*18*). Such a transition will be facilitated by the majority-spin Fermi arcs at interfaces in heterostructures since they compensate the DOS of the minority-spin electron pocket. Therefore, CoS_2 provides a prime example of a spintronic material whose performance is affected by its topologically nontrivial band structure. Note that nonmagnetic Weyl semimetals have already been successfully implemented for applications in spin-to-charge conversion and magnetic switching (*29*, *30*), and theoretically, proposals have highlighted the importance of topological Fermi arcs for interfacial spin accumulation (*31*). We therefore expect that our results will inform the design of future spintronic prototypes that use magnetic Weyl-semimetals, for instance, for spin-to-charge conversion (*11*). There may be magnetic domains on the sample surface that are smaller than the size of our beamspot (diameter of 50 to 70 μm), but on the basis of our ab initio calculations, we believe that the direction of the magnetization vector will have a negligible effect on the interpretation of the Fermi arc structure. This is because spin-orbit coupling is relatively small in CoS_2, and its inclusion has only a negligible effect on the band dispersion in our ab initio calculations (see the Supplementary Materials for further discussion). CoS_2 is also known as a good catalyst, e.g., for the hydrogen evolution reaction (*32*), and it has recently been speculated that Fermi arcs in Pt- and Pd-based chiral topological semimetals (*33*, *34*) may play a role in catalysis due to their d-electron character and their robustness against hydrogen passivation (*35*, *36*). Since the Fermi arcs in CoS_2 are also derived from bulk bands of d orbital character (see the Supplementary Materials), they may contribute to the catalytic performance of CoS_2.

Downloaded from http://advances.sciencemag.org/ on April 17, 2021

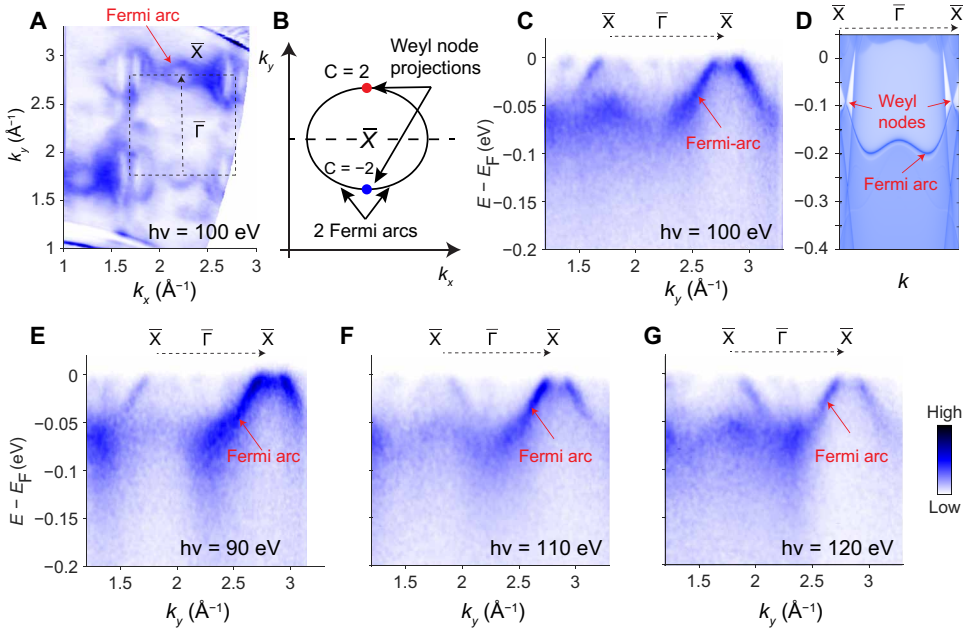

Fig. 4. Surface state structure on the (100) surface. (**A**) Experimental Fermi surface measured on the (100) cleavage plane with photon energy hv = 100 eV and linear-horizontal polarization. The dashed black line indicates the boundary of the surface Brillouin zone, and the black dashed arrow indicates the momentum direction of the line cuts shown in (C) to (F). (**B**) Illustration of the Fermi arcs and Weyl point projections in the vicinity of the surface Brillouin zone boundary (black dashed line) at the $\bar{X}$ point. Red and blue dots indicate Weyl point projections, and black arrows indicate Fermi arc positions. (**C**) Experimental band dispersion of the Fermi arc surface states along the line cut shown in (A). The photon energy used here was hv = 100 eV and the polarization was linear-horizontal. (**D**) Calculated surface state dispersion along the same momentum direction as the experimental line cuts. (**E** to **G**) Same as in (B) but for photon energies of 90, 110, and 120 eV.

MATERIALS AND METHODS

Sample growth

Single crystals of CoS_2 were synthesized using chemical vapor transport. The elements cobalt (200 mg, 1 eq, 99.5%; Sigma-Aldrich) and sulfur (217 mg, 2 eq, 99.5%; Alfa Aesar) were mixed with 50 mg of iodine (99.999%; Sigma Aldrich) and sealed in an evacuated quartz glass ampoule. The ampoule was slowly (within 12 hours) heated to 1000°C and kept there for 140 hours. The growth was along a natural temperature gradient of a tube furnace. An increase in crystal size can be accomplished using an additional slow cooling step from 1000° to 800°C in 100 hours.

ARPES measurements

SX-ARPES measurements were performed at the SX-ARPES endstation (*37*) of the ADRESS beamline (*38*) at the Swiss Light Source, Switzerland, with a SPECS analyzer with an angular resolution of 0.1°. The photon energy varied from 350 to 1000 eV, and the combined energy resolution ranged between 50 and 150 meV. The temperature during sample cleaving and measurements was below 20 K, and the pressure was lower than 1×10^{-10} mbars. The increase of the photoelectron mean free path in the soft x-ray energy range results, by the Heisenberg uncertainty principle, in a higher k_z resolution of the ARPES experiment compared to measurements at lower photon energies (*39*), which was critical to measure the bulk band structure of CoS_2.

VUV-ARPES measurements were performed at the high-resolution ARPES branch line of the beamline I05 at the Diamond Light Source, UK (*40*). Measurements at the high-resolution branch were performed with a Scienta R4000 analyzer, and a photon energy range between 90 and 130 eV, at a temperature below 20 K. Measurements in the VUV-ARPES regime are more surface sensitive than SX-ARPES and therefore most suitable to image the Fermi arcs in CoS_2.

Ab initio calculations

We used density functional theory as implemented in the Vienna Ab Initio Simulation Package. For the GGA calculations, the exchange correlation term is described according to the Perdew-Burke-Ernzerhof prescription together with projected augmented wave (PAW) pseudopotentials, while for the LSDA, the exchange correlation term is described according to the Dudarev simplified, rotationally invariant approach, together with PAW pseudopotentials. The kinetic energy cutoff was set to 400 eV. For the self-consistent calculation, a grid of $7 \times 7 \times 7$ k points was used. For DOS calculation, a grid of $11 \times 11 \times 11$ k points was used, with 1000 energy points. The spectral function of the Fermi surfaces shown in Figs. 2 and 3 was computed with the programs Wannier90 (*41*) and WannierTools (*42*). Using ab initio calculation of bands, we constructed maximally localized Wannier functions considering d orbitals for cobalt sites and p orbitals for sulfur sites using the Wannier90 software (*41*). We computed an effective tight-binding model that accurately reproduces the band structure of the bulk system. We then computed the surface spectrum by the method of iterative Green's function as implemented in WannierTools (*42*) software for a slab of 50 unit cells.

SUPPLEMENTARY MATERIALS

Supplementary material for this article is available at http://advances.sciencemag.org/cgi/content/full/6/51/eabd5000/DC1

REFERENCES AND NOTES

1. Y. Fan, P. Upadhyaya, X. Kou, M. Lang, S. Takei, Z. Wang, J. Tang, L. He, L. T. Chang, M. Montazeri, G. Yu, W. Jiang, T. Nie, R. N. Schwartz, Y. Tserkovnyak, K. L. Wang, Magnetization switching through giant spin–orbit torque in a magnetically doped topological insulator heterostructure. *Nat. Mater.* **13**, 699–704 (2014).

Downloaded from http://advances.sciencemag.org/ on April 17, 2021

2. A. R. Mellnik, J. S. Lee, A. Richardella, J. L. Grab, P. J. Mintun, M. H. Fischer, A. Vaezi, A. Manchon, E. A. Kim, N. Samarth, D. C. Ralph, Spin-transfer torque generated by a topological insulator. *Nature* **511**, 449–451 (2014).
3. M. Jamali, J. S. Lee, J. S. Jeong, F. Mahfouzi, Y. Lv, Z. Zhao, B. K. Nikolić, K. A. Mkhoyan, N. Samarth, J. P. Wang, Giant spin pumping and inverse spin hall effect in the presence of surface and bulk spin−orbit coupling of topological insulator Bi_2Se_3. *Nano Lett.* **15**, 7126–7132 (2015).
4. F. Katmis, V. Lauter, F. S. Nogueira, B. A. Assaf, M. E. Jamer, P. Wei, B. Satpati, J. W. Freeland, I. Eremin, D. Heiman, P. Jarillo-Herrero, J. S. Moodera, A high-temperature ferromagnetic topological insulating phase by proximity coupling. *Nature* **533**, 513–516 (2016).
5. C. L. Kane, E. J. Mele, Quantum spin Hall effect in graphene. *Phys. Rev. Lett.* **95**, 226801 (2005).
6. B. A. Bernevig, T. L. Hughes, S.-C. Zhang, Quantum spin Hall effect and topological phase transition in HgTe quantum wells. *Science* **314**, 1757–1761 (2006).
7. X. Wan, A. M. Turner, A. Vishwanath, S. Y. Savrasov, Topological semimetal and Fermi-arc surface states in the electronic structure of pyrochlore iridates. *Phys. Rev. B* **83**, 205101 (2011).
8. D. F. Liu, A. J. Liang, E. K. Liu, Q. N. Xu, Y. W. Li, C. Chen, D. Pei, W. J. Shi, S. K. Mo, P. Dudin, T. Kim, C. Cacho, G. Li, Y. Sun, L. X. Yang, Z. K. Liu, S. S. P. Parkin, C. Felser, Y. L. Chen, Magnetic Weyl semimetal phase in a Kagomé crystal. *Science* **365**, 1282–1285 (2019).
9. I. Belopolski, K. Manna, D. S. Sanchez, G. Chang, B. Ernst, J. Yin, S. S. Zhang, T. Cochran, N. Shumiya, H. Zheng, B. Singh, G. Bian, D. Multer, M. Litskevich, X. Zhou, S. M. Huang, B. Wang, T. R. Chang, S. Y. Xu, A. Bansil, C. Felser, H. Lin, M. Z. Hasan, Discovery of topological Weyl fermion lines and drumhead surface states in a room temperature magnet. *Science* **365**, 1278–1281 (2019).
10. N. Morali, R. Batabyal, P. K. Nag, E. Liu, Q. Xu, Y. Sun, B. Yan, C. Felser, N. Avraham, H. Beidenkopf, Fermi-arc diversity on surface terminations of the magnetic Weyl semimetal $Co_3Sn_2S_2$. *Science* **365**, 1286–1291 (2019).
11. S. S.-L. Zhang, A. A. Burkov, I. Martin, O. G. Heinonen, Spin-to-charge conversion in magnetic Weyl semimetals. *Phys. Rev. Lett.* **123**, 187201 (2019).
12. A. A. Burkov, Anomalous Hall effect in Weyl metals. *Phys. Rev. Lett.* **113**, 187202 (2014).
13. C. Wang, L. Gioia, A. A. Burkov, Fractional quantum Hall effect in Weyl semimetals. *Phys. Rev. Lett.* **124**, 096603 (2020).
14. I. I. Mazin, Robust half metalicity in $Fe_xCo_{1-x}S_2$. *Appl. Phys. Lett.* **77**, 3000 (2000); https://doi.org/10.1063/1.1324720.
15. T. Shishidou, A. J. Freeman, R. Asahi, Effect of GGA on the half-metallicity of the itinerant ferromagnet CoS_2. *Phys. Rev. B* **64**, 180401 (2001).
16. C. Leighton, M. Manno, A. Cady, J. W. Freeland, L. Wang, K. Umemoto, R. M. Wentzcovitch, T. Y. Chen, C. L. Chien, P. L. Kuhns, M. J. R. Hoch, A. P. Reyes, W. G. Moulton, E. D. Dahlberg, J. Checkelsky, J. Eckert, Composition controlled spin polarization in $Co_{1-x}Fe_xS_2$ alloys. *J. Phys. Condens. Matter* **19**, 315219 (2007).
17. K. Ramesha, R. Seshadri, C. Ederer, T. He, M. A. Subramanian, Experimental and computational investigation of structure and magnetism in pyrite $Co_{1-x}Fe_xS_2$: Chemical bonding and half-metallicity. *Phys. Rev. B* **70**, 214409 (2004).
18. L. Wang, K. Umemoto, R. M. Wentzcovitch, T. Y. Chen, C. L. Chien, J. G. Checkelsky, J. C. Eckert, E. D. Dahlberg, C. Leighton, $Co_{1-x}Fe_xS_2$: A tunable source of highly spin-polarized electrons. *Phys. Rev. Lett.* **94**, 056602 (2005).
19. L. Wang, T. Y. Chen, C. L. Chien, J. G. Checkelsky, J. C. Eckert, E. D. Dahlberg, K. Umemoto, R. M. Wentzcovitch, C. Leighton, Composition controlled spin polarization in $Co_{1-x}Fe_xS_2$: Electronic, magnetic, and thermodynamic properties. *Phys. Rev. B* **73**, 144402 (2006).
20. C. Utfeld, S. R. Giblin, J. W. Taylor, J. A. Duffy, C. Shenton-Taylor, J. Laverock, S. B. Dugdale, M. Manno, C. Leighton, M. Itou, Y. Sakurai, Bulk spin polarization of $Co_{1-x}Fe_xS_2$. *Phys. Rev. Lett.* **103**, 226403 (2009).
21. A. Teruya, F. Suzuki, D. Aoki, F. Honda, A. Nakamura, M. Nakashima, Y. Amako, H. Harima, M. Hedo, T. Nakama, Y. Ōnuki, Large cyclotron mass and large ordered moment in ferromagnet CoS_2 compared with paramagnet $CoSe_2$. *J. Physical Soc. Japan* **85**, 064716 (2016).
22. L. Wang, T. Y. Chen, C. L. Chien, C. Leighton, Sulfur stoichiometry effects in highly spin polarized CoS_2 single crystals. *Appl. Phys. Lett.* **88**, 232509 (2006).
23. P. A. Dowben, R. Skomski, Are half-metallic ferromagnets half metals? (invited). *J. Appl. Phys.* **95**, 7453–7458 (2004).
24. A. Fujimori, K. Mamiya, T. Mizokawa, T. Miyadai, T. Sekiguchi, H. Takahashi, N. Môri, S. Suga, Resonant photoemission study of pyrite-type NiS_2, CoS_2 and FeS_2. *Phys. Rev. B* **54**, 16329–16332 (1996).
25. N. Wu, Y. B. Losovyj, D. Wisbey, K. Belashchenko, M. Manno, L. Wang, C. Leighton, P. A. Dowben, The electronic band structure of CoS_2. *J. Phys. Condens. Matter* **19**, 156224 (2007).
26. N. Wu, R. F. Sabirianov, W. N. Mei, Y. B. Losovyj, N. Lozova, M. Manno, C. Leighton, P. A. Dowben, The minority spin surface bands of CoS_2 (001). *J. Phys. Condens. Matter* **21**, 295501 (2009).
27. V. N. Strocov, Intrinsic accuracy in 3-dimensional photoemission band mapping. *J. Electron Spectros. Relat. Phenomena* **130**, 65–78 (2003).
28. B. Morris, V. Johnson, A. Wold, Preparation and magnetic properties of cobalt disulfide. *J. Phys. Chem. Solid* **28**, 1565–1567 (1967).
29. S. Shi, S. Liang, Z. Zhu, K. Cai, S. D. Pollard, Y. Wang, J. Wang, Q. Wang, P. He, J. Yu, G. Eda, G. Liang, H. Yang, All-electric magnetization switching and Dzyaloshinskii–Moriya interaction in WTe_2 /ferromagnet heterostructures. *Nat. Nanotechnol.* **14**, 945–949 (2019).
30. P. Li, W. Wu, Y. Wen, C. Zhang, J. Zhang, S. Zhang, Z. Yu, S. A. Yang, A. Manchon, X. X. Zhang, Spin-momentum locking and spin-orbit torques in magnetic nano-heterojunctions composed of Weyl semimetal WTe_2. *Nat. Commun.* **9**, 3990 (2018).
31. A. Johansson, J. Henk, I. Mertig, Edelstein effect in Weyl semimetals. *Phys. Rev. B* **97**, 085417 (2018).
32. M. S. Faber, R. Dziedzic, M. A. Lukowski, N. S. Kaiser, Q. Ding, S. Jin, High-performance electrocatalysis using metallic cobalt pyrite (CoS_2) micro- and nanostructures. *J. Am. Chem. Soc.* **136**, 10053–10061 (2014).
33. N. B. M. Schröter, D. Pei, M. G. Vergniory, Y. Sun, K. Manna, F. de Juan, J. A. Krieger, V. Süss, M. Schmidt, P. Dudin, B. Bradlyn, T. K. Kim, T. Schmitt, C. Cacho, C. Felser, V. N. Strocov, Y. Chen, Chiral topological semimetal with multifold band crossings and long Fermi arcs. *Nat. Phys.* **15**, 759–765 (2019).
34. N. B. M. Schröter, S. Stolz, K. Manna, F. de Juan, M. G. Vergniory, J. A. Krieger, D. Pei, T. Schmitt, P. Dudin, T. K. Kim, C. Cacho, B. Bradlyn, H. Borrmann, M. Schmidt, R. Widmer, V. N. Strocov, C. Felser, Observation and control of maximal Chern numbers in a chiral topological semimetal. *Science* **369**, 179–183 (2020).
35. Q. Yang, G. Li, K. Manna, F. Fan, C. Felser, Y. Sun, Topological engineering of Pt-group-metal-based chiral crystals toward high-efficiency hydrogen evolution catalysts. *Adv. Mater.* **32**, 1908518 (2020).
36. G. Li, C. Felser, Heterogeneous catalysis at the surface of topological materials. *Appl. Phys. Lett.* **116**, 070501 (2020).
37. V. N. Strocov, X. Wang, M. Shi, M. Kobayashi, J. Krempasky, C. Hess, T. Schmitt, L. Patthey, Soft-X-ray ARPES facility at the ADRESS beamline of the SLS: Concepts, technical realisation and scientific applications. *J Synchrotron Rad* **21**, 32–44 (2014).
38. V. N. Strocov, T. Schmitt, U. Flechsig, T. Schmidt, A. Imhof, Q. Chen, J. Raabe, R. Betemps, D. Zimoch, J. Krempasky, X. Wang, M. Grioni, A. Piazzalunga, L. Patthey, High-resolution soft x-ray beamline ADRESS at the Swiss Light Source for resonant inelastic X-ray scattering and angle-resolved photoelectron spectroscopies. *J. Synchrotron. Radiat.* **17**, 631–643 (2010).
39. V. N. Strocov, M. Shi, M. Kobayashi, C. Monney, X. Wang, J. Krempasky, T. Schmitt, L. Patthey, H. Berger, P. Blaha, Three-dimensional electron realm in VSe_2 by soft-x-ray photoelectron spectroscopy: Origin of charge-density waves. *Phys. Rev. Lett.* **109**, 086401 (2012).
40. M. Hoesch, T. K. Kim, P. Dudin, H. Wang, S. Scott, P. Harris, S. Patel, M. Matthews, D. Hawkins, S. G. Alcock, T. Richter, J. J. Mudd, M. Basham, L. Pratt, P. Leicester, E. C. Longhi, A. Tamai, F. Baumberger, A facility for the analysis of the electronic structures of solids and their surfaces by synchrotron radiation photoelectron spectroscopy. *Rev. Sci. Instrum.* **88**, 013106 (2017).
41. G. Pizzi, V. Vitale, R. Arita, S. Blügel, F. Freimuth, G. Géranton, M. Gibertini, D. Gresch, C. Johnson, T. Koretsune, J. Ibañez-Azpiroz, H. Lee, J. M. Lihm, D. Marchand, A. Marrazzo, Y. Mokrousov, J. I. Mustafa, Y. Nohara, Y. Nomura, L. Paulatto, S. Poncé, T. Ponweiser, J. Qiao, F. Thöle, S. S. Tsirkin, M. Wierzbowska, N. Marzari, D. Vanderbilt, I. Souza, A. A. Mostofi, J. R. Yates, Wannier90 as a community code: New features and applications. *J. Phys. Condens. Matter* **32**, 165902 (2020).
42. Q. Wu, S. Zhang, H.-F. Song, M. Troyer, A. A. Soluyanov, WannierTools: An open-source software package for novel topological materials. *Comput. Phys. Commun.* **224**, 405–416 (2018).
43. P. J. Brown, K.-U. Neumann, A. Simon, F. Ueno, K. R. A. Ziebeck, Magnetization distribution in CoS_2; Is it a half metallic ferromagnet? *J. Phys. Condens. Matter* **17**, 1583–1592 (2005).
44. M. Kargarian, M. Randeria, Y.-M. Lu, Are the surface Fermi arcs in Dirac semimetals topologically protected? *Proc. Natl. Acad. Sci. U.S.A.* **113**, 8648–8652 (2016).

Acknowledgments: We thank I. Mazin, M. Watson, and F. Orlandi for fruitful discussions and helpful feedback. We acknowledge the Paul Scherrer Institut, Villigen, Switzerland, for provision of synchrotron radiation beam time at beamline ADRESS of the SLS. We also acknowledge the Diamond Light Source for time on Beamline I05 under proposals SI26098 and SI20617. **Funding:** This work was supported by NSF through the Princeton Center for Complex Materials, a Materials Research Science and Engineering Center DMR-1420541, by Princeton University through the Princeton Catalysis Initiative, and by the Gordon and Betty Moore Foundation through grant GBMF9064 to L.M.S. F.d.J. acknowledges funding from the Spanish MCI/AEI through grant no. PGC2018-101988-B-C21. M.G.V. and F.J. acknowledge funding from the Basque Government through grant PIBA 2019-81. M.G.V. and I.R. acknowledge the Spanish Ministerio de Ciencia e Innovacion (grant number PID2019-109905GB-C21). N.B.M.S. was supported by Microsoft. A.B. acknowledges financial support from the Spanish Ministry of Science and Innovation (PID2019-105488GB-I00). The work of S.S.

Downloaded from http://advances.sciencemag.org/ on April 17, 2021

was supported by the Swiss National Science Foundation under grant no. 159690. D.P. acknowledges the support from the Chinese Scholarship Council. J.A.K. acknowledges support by the Swiss National Science Foundation (SNF-Grant no. 200021_165910). **Author contributions:** This project was led jointly by N.B.M.S., M.G.V., and L.M.S. N.B.M.S. performed the ARPES experiments with support from J.A.K., D.P., T.Y., S.S., and V.N.S. I.R., F.d.J., and M.G.V. performed the ab initio calculations and theoretical analysis with support from A.S. and A.B. S.K. and R.J.K. performed the sample growth and structural and magnetic characterization. T.S., P.D., T.K.K., C.C., and V.N.S. maintained the ARPES endstations and provided experimental support. The project was supervised by M.G.V. and L.M.S. All authors discussed the results and contributed to the writing of the manuscript. **Competing interests:** The authors declare that they have no competing interests. **Data and materials availability:** All data needed to evaluate the conclusions in the paper are present in the paper and/or the Supplementary Materials. Additional data related to this paper may be requested from the authors.

Submitted 24 June 2020
Accepted 5 November 2020
Published 18 December 2020
10.1126/sciadv.abd5000

Citation: N. B. M. Schröter, I. Robredo, S. Klemenz, R. J. Kirby, J. A. Krieger, D. Pei, T. Yu, S. Stolz, T. Schmitt, P. Dudin, T. K. Kim, C. Cacho, A. Schnyder, A. Bergara, V. N. Strocov, F. de Juan, M. G. Vergniory, L. M. Schoop, Weyl fermions, Fermi arcs, and minority-spin carriers in ferromagnetic CoS_2. *Sci. Adv.* **6**, eabd5000 (2020).

Downloaded from http://advances.sciencemag.org/ on April 17, 2021

Science Advances

Weyl fermions, Fermi arcs, and minority-spin carriers in ferromagnetic CoS_2

Niels B. M. Schröter, Iñigo Robredo, Sebastian Klemenz, Robert J. Kirby, Jonas A. Krieger, Ding Pei, Tianlun Yu, Samuel Stolz, Thorsten Schmitt, Pavel Dudin, Timur K. Kim, Cephise Cacho, Andreas Schnyder, Aitor Bergara, Vladimir N. Strocov, Fernando de Juan, Maia G. Vergniory and Leslie M. Schoop

Sci Adv **6** (51), eabd5000.
DOI: 10.1126/sciadv.abd5000

ARTICLE TOOLS http://advances.sciencemag.org/content/6/51/eabd5000

SUPPLEMENTARY MATERIALS http://advances.sciencemag.org/content/suppl/2020/12/14/6.51.eabd5000.DC1

REFERENCES This article cites 44 articles, 6 of which you can access for free
http://advances.sciencemag.org/content/6/51/eabd5000#BIBL

PERMISSIONS http://www.sciencemag.org/help/reprints-and-permissions

Use of this article is subject to the Terms of Service

Science Advances (ISSN 2375-2548) is published by the American Association for the Advancement of Science, 1200 New York Avenue NW, Washington, DC 20005. The title *Science Advances* is a registered trademark of AAAS.

Copyright © 2020 The Authors, some rights reserved; exclusive licensee American Association for the Advancement of Science. No claim to original U.S. Government Works. Distributed under a Creative Commons Attribution NonCommercial License 4.0 (CC BY-NC).

Downloaded from http://advances.sciencemag.org/ on April 17, 2021